Chapter 7

Group 14

7.1 The Group 14 Elements[1]

The group was once also known as the *tetrels* (from Greek *tetra* meaning *four*), stemming from the earlier naming convention of this group as Group IVA. Table 7.1 lists the derivation of the names of the Group 14 elements.

Element	**Symbol**	**Name**
Carbon	C	From the Latin *carbo* meaning *coal*
Silicon	Si	From the Latin *silicis* meaning *flints*
Germanium	Ge	From the Latin *Germania* for *Germany*
Tin	Sn	From the Anglo-Saxon and from the Latin *stannum* meaning *melts easily*
Lead	Pb	From the Anglo-Saxon, and from the Latin *plumbum* meaning *soft metal*

Table 7.1: Derivation of the names of each of the Group 14 elements.

7.1.1 Discovery

7.1.1.1 Carbon

Carbon was known in prehistory in the form of soot; while charcoal was made in Roman times (by heating wood while exclude air) and diamonds were known as early as 2500 BC in China. In 1772, Antoine Lavoisier (Figure 7.1) showed that diamonds were a form of carbon, when he burned samples of carbon and diamond and showed that both formed the same amount of carbon dioxide per gram of material. Carl Scheele (Figure 7.2) showed that graphite was a form of carbon rather a form of lead.

---

[1] This content is available online at <http://cnx.org/content/m32186/1.3/>.

Figure 7.1: French chemist and biologist Antoine-Laurent de Lavoisier (1743 – 1794).

Figure 7.2: German-Swedish pharmaceutical chemist Carl Wilhelm Scheele (1742 - 1786). Author Isaac Asimov has called him "hard-luck Scheele" because he made a number of chemical discoveries before others who are generally given the credit.

A new allotrope of carbon, fullerene, was discovered in 1985 by Robert Curl, Harry Kroto, and Richard Smalley (Figure 7.3) who subsequently shared the Nobel Prize in Chemistry in 1996. Fullerenes have been reveled to include nanostructured forms such as buckyballs and nanotubes. The renewed interest in new forms lead to the discovery of further exotic allotropes, including glassy carbon, and the realization that *amorphous carbon* is not amorphous.

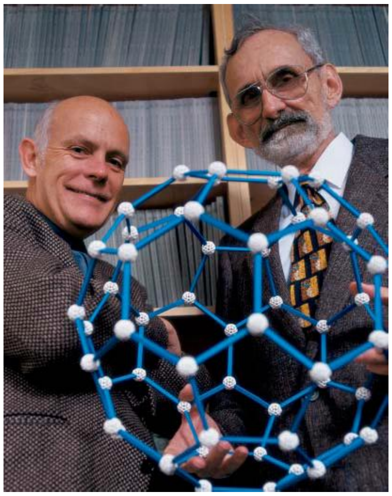

Figure 7.3: Rice University chemists Richard E. Smalley (1943 - 2005) and Robert F. Curl (1933 -).

7.1.1.2 Silicon

Silicon was first identified by Antoine Lavoisier (Figure 7.1) in 1787 as a component of flints, and was later mistaken by Humphry Davy (Figure 7.4) for a compound rather than an element. In 1824, Berzelius (Figure 7.5) prepared amorphous silicon by the reaction of potassium with silicon tetrafluoride, (7.1)

$$SiCl_4 + 4\,K \rightarrow Si + 4\,KCl \tag{7.1}$$

Figure 7.4: British chemist and inventor Sir Humphry Davy FRS (1778 - 1829).

Figure 7.5: Swedish chemist Jöns Jacob Berzelius (1779 – 1848).

7.1.1.3 Germanium

In 1869 Dmitri Mendeleev (Figure 7.6) predicted the existence of several unknown elements, including ekasilicon (Es) between silicon and tin.

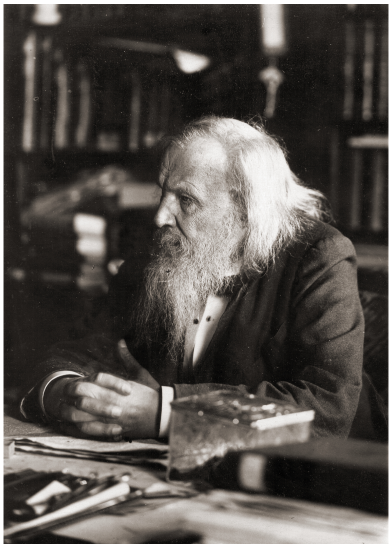

Figure 7.6: Russian chemist and inventor Dmitri Ivanovich Mendeleev (1834 – 1907).

In 1885 a new mineral (named *argyrodite* because of its high silver content) was found in a mine near Freiberg, Saxony. Clemens Winkler (Figure 7.7) isolated Mendeleev's missing element. He originally was going to name neptunium because like this element, because like ekasilicon, the planet Neptune had been preceded by mathematical prediction of its existence. However, the name neptunium had already been given to an element and so Winkler named the new metal germanium in honor of his fatherland.

Figure 7.7: German chemist Clemens Alexander Winkler (1838 –1904).

Winkler was able to isolate sufficient germanium from 500 kg of ore to determine a number properties, including an atomic weight of 72.32 g/mol by analyzing pure germanium tetrachloride ($GeCl_4$). Winkler prepared several new compounds of germanium, including the fluorides, chlorides, sulfides, germanium dioxide, and tetraethylgermane ($Ge(C_2H_5)_4$). The physical data from these compounds, corresponded with Mendeleev's predictions (Table 7.2).

Property	**Ekasilicon**	**Germanium**
Atomic mass	72	72.59
Density (g/cm^3)	5.5	5.35
Melting point (°C)	High	947
Color	Gray	Gray
Oxide type	Refractory dioxide	Refractory dioxide
Oxide density (g/cm^3)	4.7	4.7
Oxide activity	Feebly basic	Feebly basic
Chloride boiling point (°C)	Under 100	86 ($GeCl_4$)
Chloride density (g/cm^3)	1.9	1.9

Table 7.2: Properties predicted for ekasilicon compared those determined for germanium.

7.1.1.4 Tin

Tin is one of the earliest metals known. When the addition of about 5% tim to molten copper produced an alloy (bronze) that was easier to work and much harder than copper, it revolutionized civilization. The widespread use of bronze to make tools and weapons became part of what archaeologists call the Bronze Age. The Bronze Age arrived in Egypt, Mesopotamia and the Indus Valley culture by around 3000 BC.

7.1.1.5 Lead

Lead has been commonly used for thousands of years because of its ease of extraction, and its ease of smelting. Lead beads dating back to 6400 BC have been found in Çatalh*öyü*k in modern-day Turkey, while lead was used during the Bronze Age.

7.1.2 Abundance

Carbon and silicon are amongst the most abundant elements (Table 7.3). Silicon is the second most abundant element (after oxygen) in the Earth's crust, making up 28% of the crust. Carbon is the fourth most abundant chemical element in the universe after hydrogen, helium, and oxygen. In combination with oxygen in carbon dioxide, carbon is found in the Earth's atmosphere (in quantities of approximately 810 gigatonnes) and dissolved in all water bodies (approximately 36,000 gigatons). Around 1,900 gigatons are present in the biosphere. Hydrocarbons (such as coal, petroleum, and natural gas) contain carbon amounts to around 900 gigatons. Natural diamonds occur in the rock kimberlite, found in ancient volcanic "necks," or "pipes". Most diamond deposits are in Africa but there are also deposits in Canada, the Russian Arctic, Brazil, and Australia.

Element	**Terrestrial abundance (ppm)**
C	480 (Earth's crust), 28 (sea water), 350 (atmosphere CO_2), 1.6 (atmosphere, CH_4), 0.25 (atmosphere, CO)
Si	28,000 (Earth's crust), 2 (sea water)
Ge	2 (Earth's crust), 1 (soil), 5 x 10^{-7} (sea water)
Sn	2 (Earth's crust), 1 (soil), 4 x 10^{-6} (sea water)
Pb	14 (Earth's crust), 23 (soil), 2 x 10^{-6} (sea water)

Table 7.3: Abundance of Group 14 elements.

7.1.3 Isotopes

Table 7.4 summarizes the naturally occurring isotopes of the Group 14 elements.

Isotope	**Natural abundance (%)**
Carbon-12	98.9
Carbon-13	1.1
Carbon-14	trace
Silicon-28	92.23
Silicon-29	4.67
Silicon -30	3.1
Germanium-70	21.23
Germanium-72	27.66
Germanium-73	7.73
Germanium-74	35.94
Germanium-76	7.44
Tin-112	0.97
Tin-114	0.66
Tin-115	0.34
Tin-116	14.54
Tin-117	7.68
Tin-118	24.22
Tin-119	8.59
Tin-120	32.58
Tin-122	4.63
Tin-124	5.79
Lead-204	1.4
Lead-24.1	24.1
Lead-207	22.1
Lead-208	52.4

Table 7.4: Abundance of the major isotopes of the Group 14 elements.

Although radioactive, carbon-14 is formed in upper layers of the troposphere and the stratosphere, at altitudes of 9–15 km. Thermal neutrons produced by cosmic rays collide with the nuclei of nitrogen-14, forming carbon-14 and a proton. Because of its relatively short half-life of 5730 years, carbon-14 is absent in ancient rocks, but is incorporated in living organisms.

7.1.3.1 Carbon dating

Carbon dating is a process whereby the age of a material that contains carbon can be determined by comparing the decay rate of that material with that of living material.

Carbon-14 has a half life ($t_{1/2}$) of 5.73 x 10^3 years for its decay to nitrogen-14 by the loss of a β particle, (7.2).

$$ {}^{14}_{6}\mathrm{C} \rightarrow {}^{14}_{7}\mathrm{N} + {}^{0}_{-1}\mathrm{e} \qquad (7.2) $$

The rate of radioactive decay can be expressed as a rate constant (k):

$$k = \frac{\ln[2]}{t_{1/2}} = \frac{0.693}{t_{1/2}} \tag{7.3}$$

For carbon-14, using (7.3),

$$k = \frac{0.693}{5.73 \text{ x } 10^{3}} = 1.21 \text{ x } 10^{-4} \text{ year}^{-1} \tag{7.4}$$

In 1947 samples of the Dead Sea Scrolls were analyzed by carbon dating. It was found that the carbon-14 present had an activity of d/min.g (where d = disintegration); by contrast in living material the activity is 14 d/min.g. Thus,

$$\ln \frac{14}{11} = (1.21 \text{ x } 10^{-4})\, t \tag{7.5}$$

$$t = \frac{\ln 1.272}{1.21 \text{ x } 10^{-4}} = 2.0 \text{ x } 10^{3} \text{ years} \tag{7.6}$$

From the measurement performed in 1947 the Dead Sea Scrolls were determined to be 2000 years old giving them a date of 53 BC, and confirming their authenticity. This discovery is in contrast to the carbon dating results for the Turin Shroud that was supposed to have wrapped Jesus' body. Carbon dating has shown that the cloth was made between 1260 and 1390 AD. Thus, the Turin Shroud is clearly a fake having been made over a thousand years after its supposed manufacture.

7.1.4 Industrial production

Due to the industrial importance of carbon and silicon, as well as the wide range of fullerene materials, the production of these elements is discussed elsewhere. However, the diamond supply chain is controlled by a limited number of commercial concerns, the largest of which is DeBeers in London (Figure 7.8). Diamonds make up only a very small fraction of ore bearing rock. The ore is crushed and subsequently the particles are sorted by density. Diamonds are located in the diamond-rich fraction by X-ray fluorescence, after which the final sorting steps are done by hand.

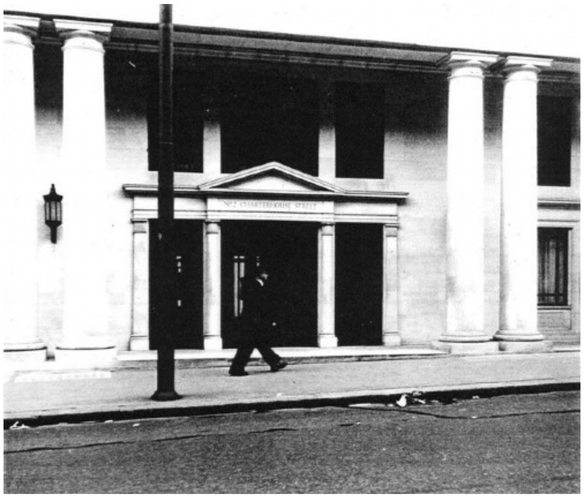

Figure 7.8: The Charterhouse Street Entrance of the offices of De Beers in London, are the venue for the 10 sights that are held during the year. Sightholders, both manufacturers (of polished diamonds) and dealers (in rough diamonds), meet in London, once every 5 weeks, 10 times a year, to inspect their diamond allocations.

Germanium ore concentrates are mostly sulfidic, e.g., as an impurity in zinc blende. They are converted to the oxides by heating under air (roasting), (7.7).

$$GeS_2 + 3\,O_2 \rightarrow GeO_2 + 2\,SO_2 \quad (7.7)$$

Part of the germanium ends up in the dust produced during this process, while the rest is converted to germanates which are leached together with the zinc by sulfuric acid. After neutralisation the germanium and other metals are precipitated (leaving the Zn^{2+} in solution). Germanium dioxide is obtained as a precipitate and converted with chlorine gas or hydrochloric acid to germanium tetrachloride, (7.8) (7.9), which has a low boiling point and can be purified by distillation.

$$GeO_2 + 4\,HCl \rightarrow GeCl_4 + 2\,H_2O \quad (7.8)$$

$$GeO_2 + 2\,Cl_2 \rightarrow GeCl_4 + O_2 \quad (7.9)$$

The germanium tetrachloride is hydrolyzed to the give pure oxide (GeO_2), which is then converted to germanium glass for the semiconductor industry, (7.10). Germanium used in steel production and other applications that do not require the high purity is produced by reduction with carbon, (7.11).

$$GeO_2 + 4\,H_2 \rightarrow Ge + 2\,H_2O \quad (7.10)$$

$$GeO_2 + C \rightarrow Ge + CO_2 \quad (7.11)$$

Tin is mined and subsequently smelted, and its production has changed little. In contrast, lead-rich ores contain less than 10% lead, but ores containing as little as 3% lead can be economically exploited. Ores are crushed and concentrated to 70%. Sulfide ores are roasted, producing lead oxide and a mixture of sulfates and silicates of lead. Lead oxide from the roasting process is reduced in a coke-fired blast furnace. This converts most of the lead to its metallic form. Metallic lead that results from the roasting and blast furnace processes still contains significant contaminants of arsenic, antimony, bismuth, zinc, copper, silver, and gold. The melt is treated in a reverberatory furnace (Figure 7.9) with air, steam, and sulfur, which oxidizes the contaminants except silver, gold, and bismuth.

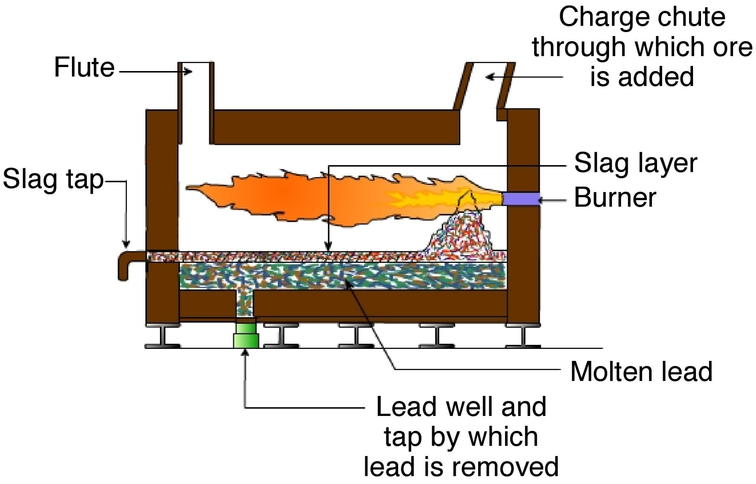

Figure 7.9: Schematic of a reverberatory furnace.

7.1.5 Physical properties

Table 7.5 provides a summary of the physical properties of the Group 14 elements.

Element	**Mp (°C)**	**Bp (°C)**	**Density (g/cm^3)**
C	642 (sublimes)		2.267 (graphite), 3.515 (diamond), 1.8 - 2.1 (amorphous)
Si	1414	3265	2.3290
Ge	938	2833	5.323
Sn	232	2602	7.365 (white), 5.769 (gray)
Pb	327	1749	11.34

Table 7.5: Selected physical properties of the Group 14 elements.

7.1.5.1 Cubic structure

The elements carbon through tin (in its α form) all exist in diamond cubic structure (Figure 7.10a), while lead crystallizes in a cubic close packed structure (Figure 7.10b). As expected the lattice parameter (a) increases with increased atomic radius (Table 7.6). The switch from diamond cubic to close packed cubic may be rationalized by the relative atomic sizes. The diamond cubic structure comprises of two interpenetrating cubic close packed lattices. As the atomic size increases large interstitial vacancies would result, resulting in an unfavorable low-density structure.

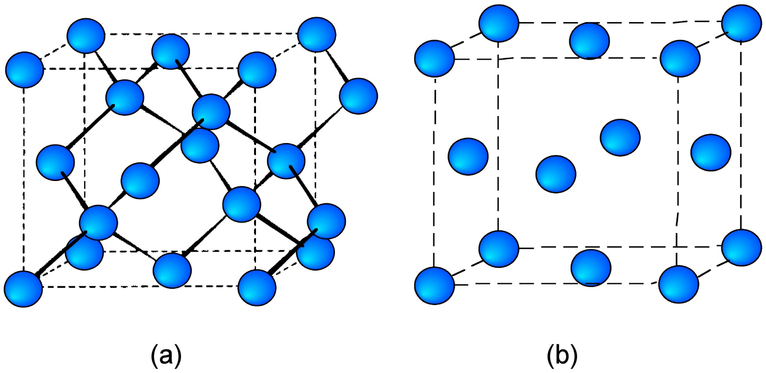

Figure 7.10: Unit cell structure of (a) the diamond cubic lattice showing the two interpenetrating face-centered cubic lattices, and (b) the cell of cubic close packed structure for comparison.

Element	**Structure**	**a (Å)**	**Atomic radius (Å)**
C	diamond cubic	3.566	0.70
Si	diamond cubic	5.431	1.10
Ge	diamond cubic	5.657	1.25
α-Sn (gray)	diamond cubic	6.489	1.45
Pb	cubic close packed	4.951	1.80

Table 7.6: Lattice parameter and crystal density for Group 14 elements.

7.2 Carbon

7.2.1 Carbon Black: From Copying to Communication[2]

It is a commonly held fallacy that James Watt (Figure 7.11) was the inventor of the steam engine. This actually honor belongs to Thomas Newcomen (Figure 7.12). Watt's actual achievement was to improve Newcomen's design of a steam pump. While Watt was working in the repair shop at the University of Glasgow he was fixing a Newcomen pump when he developed several key improvements on the original design.

---

[2] This content is available online at <http://cnx.org/content/m32173/1.1/>.

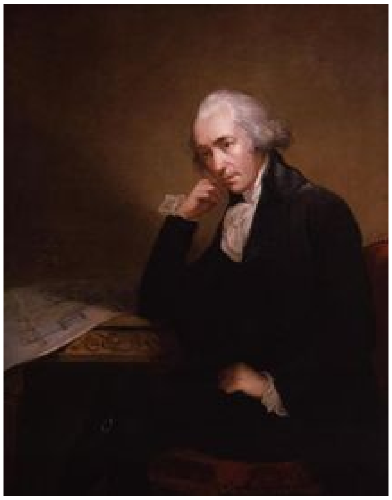

Figure 7.11: Scottish inventor and mechanical engineer James Watt FRS (1736 –1819).

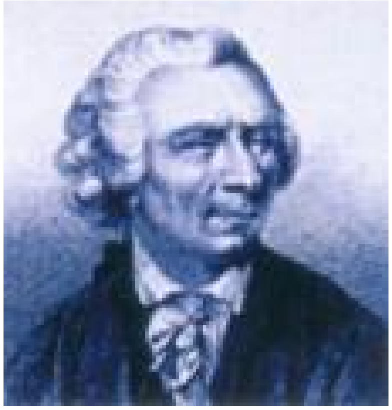

Figure 7.12: English ironmonger and inventor of the steam engine Thomas Newcomen (1664 - 1729).

The reason for Watt's success was that Britain was going through a major industrial boom and was in need of significant quantities of raw material including coal. Many of the coalmines, especially those in Devon were prone to flooding. Unfortunately, Newcomen's engine (which was actually a steam pump) could not pump the water out fast enough, whereas Watt's engine was powerful enough to drain the mines. As a result Watt's career as a manufacturer was assured. However, Watt did not see the full potential of his invention, this was left to an employee of his, William Murdock (Figure 7.13), whose invention of the gearing to allow the steam engine to be used for powering machinery.

Figure 7.13: Scottish engineer and inventor William Murdock (1754 - 1839).

One outcome that Watt found from his increased business was an increase in paperwork! While he was living in Redruth, Cornwall, close to where many of the mines were situated he told a friend that he was having “excessive difficulty in finding intelligent managing clerks”. In 1780 Watt solved his paperwork problems by inventing the first method of making copies. This was the subject of a Patent entitled “A new method of copying letters and writing expeditiously”. Watt's invention involved making ink out of gum Arabic and carbon black.

> NOTE: Gum arabic, also known as *gum acacia*, is a natural gum made of the hardened sap taken from two species of the acacia tree; *acacia senegal* and *acacia seyal*. Carbon black is a form of amorphous carbon that has a high surface area to volume ratio it is commonly produced by the incomplete combustion of heavy petroleum products such as coal tar.

Watt's ink would stay wet for 24 hours. Writing with the ink and then pressing the result against another piece of paper created a copy. Initially there was great resistance to the copy paper. In particular banks believed that this form of copying could result in forgeries. However, by the end of its first year on sale, Watt sold over 200 examples. The real commercial push came after Watt demonstrated his process to the House of Parliament. The resultant consternation amongst the Members of Parliament resulted in their having to be reminded that Parliament was still in session! By 1785 copies were in general use, however, Cyrus P. Dalkin made the biggest advance in 1823. By using a mixture of carbon black and hot paraffin wax the back of a piece of paper was coated. The carbon black was transferred to another piece of paper underneath by the pressure of the pen. Dalkin had created *carbon copies*. Both Ralph Wedgwood in England and Pellegrino Turri in Italy had developed forms of carbon paper between 1806 and 1808, but it was Dalkin's version of carbon copy paper that found usage (Figure 7.14).

Figure 7.14: Modern carbon paper.

Initially there was almost no market for this new carbon copy paper, until in 1868 when American Lebbeus Rogers was talking part in a balloon ascent. Rogers was an owner of biscuit and greengrocer companies, and was intrigued when a reporter for the Associated Press who was interviewing him used Dalkin's carbon paper. Rogers gave up his biscuit business and founded a firm to sell carbon paper. In 1873 he talked with E. Remington and Sons the typewriter manufacturer, and it was this application that created a success out of the carbon paper business.

> NOTE: The term "CC" commonly used in e-mail programs today grew from the use of carbon paper and means *carbon copy*.

Interestingly, carbon black is still used today in modern photocopiers and laser printers. One of the attributes that allow its use is the ability for carbon black particles to become charged. This is related to another application of carbon black in early communications: its ability to conduct electric, and the changes that occur as a function of external pressure.

While Alexander Graham Bell was the first to be awarded a US patent for the electric telephone in March 1876, it was an invention by Thomas Edison (Figure 7.15) that provided significant improvements. Early telephones relied on a metal diaphragm that was attached to an electromagnet. Speaking into the metal diaphragm caused its vibration, which in tern vibrated the electromagnetic and hence created a current. Unfortunately, the current was very low and subsequent clarity was poor. Between 1877 and 1878 Edison investigated methods to improve the clarity of the signal. The key development was the carbon microphone (Figure 7.16).

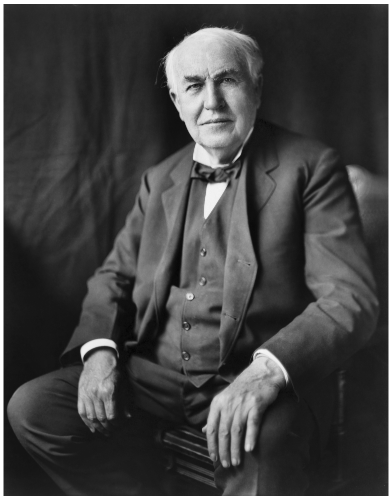

Figure 7.15: American inventor, scientist and businessman Thomas Alva Edison (1847 –1931).

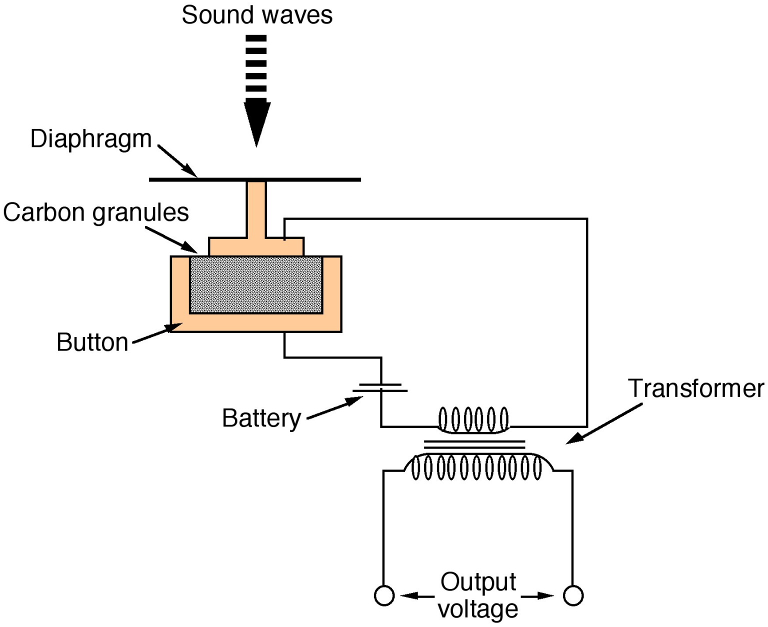

Figure 7.16: A schematic of a simple carbon "button" microphone.

The carbon microphone, also known as a carbon button microphone consisting of two metal plates separated by granules of carbon. One plate faces outward and acts as a diaphragm. When sound waves strike this plate, the pressure on the granules changes, which in turn changes the electrical resistance between the plates. A direct current is passed from one plate to the other, and the changing resistance results in a changing current, which can be passed through a telephone system. The carbon microphone was used in all telephones until the 1980s.

It was one of Edison's researchers, Edward Acheson (Figure 7.17) whose discovery allowed for the extension of communication on a global scale. While trying to make artificial diamonds, Acheson began mixing clay and coke (carbon) at very high temperatures. In an electric furnace at high temperatures he found hexagonal crystals of silicon carbide (SiC) attached to the carbon electrode. He called this material carborundum. When, by mistake, he overheated the mixture to 4150 °C he found that the silicon evaporated (boiling point 3265 °C) leaving pure and highly crystalline carbon: graphite.

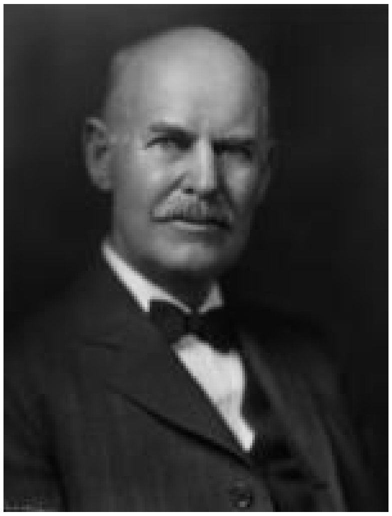

Figure 7.17: American chemist Edward Goodrich Acheson (1856 – 1931).

Graphite is a natural mineral normally associated with other minerals, although an enormous deposit of graphite was discovered in Cumbria, England, which the locals found very useful for marking sheep! Graphite was named by Abraham Werner (Figure 7.18) in 1789 from the Greek *graphein* meaning *to draw/write* due to its use in pencils. However, its use was limited due to the cost. The ability to manufacture high purity graphite resulted in its use in electrodes, dynamo brushes, and batteries. The most terrifying application of graphite was as a result of a material problem associated with the V-2 rocket built by Germany during the Second World War.

Figure 7.18: German geologist Abraham Gottlob Werner (1749 –1817).

The V-2 rockets or Vergeltungswaffen-2 (vengeance weapon-2) was 47 feet long, and reached 3,600 mph with an altitude of 300,000 feet (Figure 7.19). In order to control the direction of flight the V-2 was guided by four external rudders on the tail fins, and four internal vanes at the exit of the jet (Figure 7.20). These vanes were made of graphite, it being the only material that would survive the extreme temperatures.

Figure 7.19: A V-2 rocket at the Peenem*ü*nde Museum.

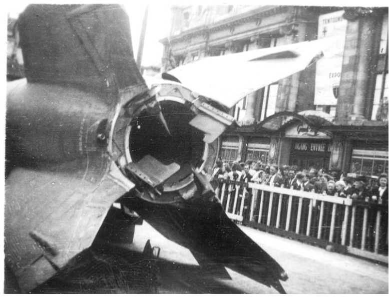

Figure 7.20: View of the V-2 rocket showing the graphite vanes for directional control.

Of course it was as a result of the same German scientists who worked on the V-2, working for NASA, that allowed rockets of sufficient power to escape the Earth's gravitational pull and send man to the moon, and position many of the satellites that are now vital for global communication.

7.2.2 Carbon Nanomaterials

7.2.2.1 Fullerenes and Nanotubes[3]

7.2.2.1.1 Introduction

Although nanomaterials had been known for many years prior to the report of C_{60} the field of nanoscale science was undoubtedly founded upon this seminal discovery. Part of the reason for this explosion in nanochemistry is that while carbon materials range from well-defined nano sized molecules (i.e., C_{60}) to tubes with lengths of hundreds of microns, they do not exhibit the instabilities of other nanomaterials as a result of the very high activation barriers to their structural rearrangement. As a consequence they are highly stable even in their unfunctionalized forms. Despite this range of carbon nanomaterials possible they exhibit common reaction chemistry: that of organic chemistry.

The previously unknown allotrope of carbon: C_{60}, was discovered in 1985, and in 1996, Curl, Kroto, and Smalley were awarded the Nobel Prize in Chemistry for the discovery. The other allotropes of carbon are graphite (sp^2) and diamond (sp^3). C_{60}, commonly known as the "buckyball" or "Buckminsterfullerene", has a spherical shape comprising of highly pyramidalized sp^2 carbon atoms. The C_{60} variant is often compared to the typical soccer football, hence buckyball. However, confusingly, this term is commonly used for higher derivatives. Fullerenes are similar in sheet structure to graphite but they contain pentagonal (or sometimes heptagonal) rings that prevent the sheet from being planar. The unusual structure of C_{60} led to the introduction of a new class of molecules known as fullerenes, which now constitute the third allotrope of carbon. Fullerenes are commonly defined as "any of a class of closed hollow aromatic carbon compounds that are made up of twelve pentagonal and differing numbers of hexagonal faces."

The number of carbon atoms in a fullerene range from C_{60} to C_{70}, C_{76}, and higher. Higher order fullerenes include carbon nanotubes that can be described as fullerenes that have been stretched along a rotational axis to form a tube. As a consequence of differences in the chemistry of fullerenes such as C_{60} and C_{70} as compared to nanotubes, these will be dealt with separately herein. In addition there have also been reports of nanohorns and nanofibers, however, these may be considered as variations on the general theme. It should be noted that fullerenes and nanotubes have been shown to be in flames produced by hydrocarbon combustion. Unfortunately, these naturally occurring varieties can be highly irregular in size and quality, as well as being formed in mixtures, making them unsuitable for both research and industrial applications.

---

[3] This content is available online at <http://cnx.org/content/m22580/1.4/>.

7.2.2.1.2 Fullerenes

Carbon-60 (C_{60}) is probably the most studied individual type of nanomaterial. The spherical shape of C_{60} is constructed from twelve pentagons and twenty hexagons and resembles a soccer ball (Figure 7.21a). The next stable higher fullerene is C_{70} (Figure 7.21b) that is shaped like a rugby or American football. The progression of higher fullerenes continues in the sequence C_{74}, C_{76}, C_{78}, etc. The structural relationship between each involves the addition of six membered rings. Mathematically (and chemically) two principles define the existence of a stable fullerene, i.e., Euler's theorem and isolated pentagon rule (IPR). Euler's theorem states that for the closure of each spherical network, n ($n \geq 2$) hexagons and 12 pentagons are required while the IPR says no two pentagons may be connected directly with each other as destabilization is caused by two adjacent pentagons.

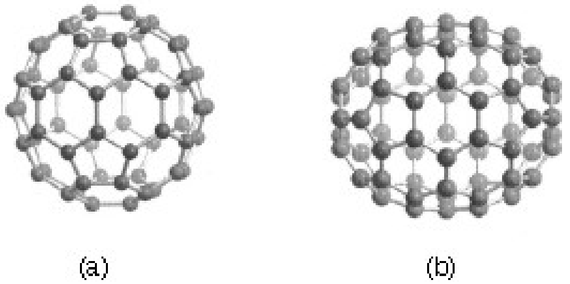

Figure 7.21: Molecular structures of (a) C_{60} and (b) C_{70}.

Although fullerenes are composed of sp^2 carbons in a similar manner to graphite, fullerenes are soluble in various common organic solvents. Due to their hydrophobic nature, fullerenes are most soluble in CS_2 (C_{60} = 7.9 mg/mL) and toluene (C_{60} = 2.8 mg/mL). Although fullerenes have a conjugated system, their aromaticity is distinctive from benzene that has all C-C bonds of equal lengths, in fullerenes two distinct classes of bonds exist. The shorter bonds are at the junctions of two hexagons ([6, 6] bonds) and the longer bonds at the junctions of a hexagon and a pentagon ([5,6] bonds). This difference in bonding is responsible for some of the observed reactivity of fullerenes.

7.2.2.1.2.1 Synthesis of fullerenes

The first observation of fullerenes was in molecular beam experiments at Rice University. Subsequent studies demonstrated that C_{60} it was relatively easy to produce grams of fullerenes. Although the synthesis is relatively straightforward fullerene purification remains a challenge and determines fullerene's commercial price. The first method of production of measurable quantities of fullerenes used laser vaporization of carbon in an inert atmosphere, but this produced microscopic amounts of fullerenes. Laboratory scales of fullerene are prepared by the vaporization of carbon rods in a helium atmosphere. Commercial production ordinarily employs a simple ac or dc arc. The fullerenes in the black soot collected are extracted in toluene and purified by liquid chromatography. The magenta C_{60} comes off the column first, followed by the red C_{70}, and other higher fullerenes. Even though the mechanism of a carbon arc differs from that of a resistively heated carbon rod (because it involves a plasma) the He pressure for optimum C_{60} formation is very similar.

A ratio between the mass of fullerenes and the total mass of carbon soot defines fullerene yield. The yields determined by UV-Vis absorption are approximately 40%, 10-15%, and 15% in laser, electric arc, and solar processes. Interestingly, the laser ablation technique has both the highest yield and the lowest productivity and, therefore, a scale-up to a higher power is costly. Thus, fullerene commercial production is a challenging task. The world's first computer controlled fullerene production plant is now operational at the MER Corporation, who pioneered the first commercial production of fullerene and fullerene products.

7.2.2.1.2.2 Endohedral fullerenes

Endohedral fullerenes are fullerenes that have incorporated in their inner sphere atoms, ions or clusters. Endohedral fullerenes are generally divided into two groups: endohedral metallofullerenes and non-metal doped fullerenes. The first endohedral metallofullerenes was called La@C_{60}. The @ sign in the name reflects the notion of a small molecule trapped inside a shell.

Doping fullerenes with metals takes place *in-situ* during the fullerene synthesis in an arc reactor or via laser evaporation. A wide range of metals have been encased inside a fullerene, i.e., Sc, Y, La, Ce, Ba, Sr, K, U, Zr, and Hf. Unfortunately, the synthesis of endohedral metallofullerenes is unspecific because in addition a high yield of unfilled fullerenes, compounds with different cage sizes are prepared (e.g., La@C_{60} or La@C_{82}). A characteristic of endohedral metallofullerenes is that electrons will transfer from the metal atom to the fullerene cage and that the metal atom takes a position off-center in the cage. The size of the charge transfer is not always simple to determine, but it is usually between 2 and 3 units (e.g., La_2@C_{80}) but can be as high as 6 electrons (e.g., Sc_3N@C_{80}). These anionic fullerene cages are very stable molecules and do not have the reactivity associated with ordinary empty fullerenes (see below). This lack of reactivity is utilized in a method to purify endohedral metallofullerenes from empty fullerenes.

The endohedral He@C_{60} and Ne@C_{60} form when C_{60} is exposed to a pressure of around 3 bar of the appropriate noble gases. Under these conditions it was possible to dope 1 in every 650,000 C_{60} cages with a helium atom. Endohedral complexes with He, Ne, Ar, Kr and Xe as well as numerous adducts of the He@C_{60} compound have also been proven with operating pressures of 3000 bars and incorporation of up to 0.1 % of the noble gases. The isolation of N@C_{60}, N@C_{70} and P@C_{60} is very unusual and unlike the metal derivatives no charge transfer of the pnictide atom in the center to the carbon atoms of the cage takes place.

7.2.2.1.2.3 Chemically functionalized fullerenes

Although fullerenes have a conjugated aromatic system all the carbons are quaternary (i.e., containing no hydrogen), which results in making many of the characteristic substitution reactions of planar aromatics impossible. Thus, only two types of chemical transformations exist: redox reactions and addition reactions. Of these, addition reactions have the largest synthetic value. Another remarkable feature of fullerene addition chemistry is the thermodymics of the process. Since the sp^2 carbon atoms in a fullerene are paramidalized there is significant strain energy. For example, the strain energy in C_{60} is *ca* 8 kcal/mol, which is 80% of its heat of formation. So the relief of this strain energy leading to sp^3 hybridized C atoms is the major driving force for addition reactions (Figure 7.22). As a consequence, most additions to fullerenes are exothermic reactions.

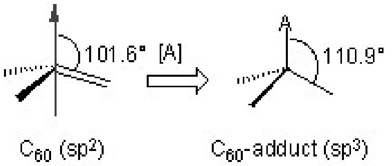

Figure 7.22: Strain release after addition of reagent A to a pyramidalize carbon of C_{60}.

Cyclic voltammetry (CV) studies show that C_{60} can be reduced and oxidized reversibly up to 6 electrons with one-electron transfer processes. Fulleride anions can be generated by electrochemical method and then be used to synthesize covalent organofullerene derivatives. Alkali metals can chemically reduce fullerene in solution and solid state to form M_xC_{60} (x = 3 - 6). C_{60} can also be reduced by less electropositive metals like mercury to form C_{60}^- and C_{60}^{2-}. In addition, salts can also be synthesized with organic molecules, for example $[TDAE^+][C_{60}^-]$ possesses interesting electronic and magnetic behavior.

Geometric and electronic analysis predicted that fullerene behaves live an electro-poor conjugated polyolefin. Indeed C_{60} and C_{70} undergo a range of nucleophilic reactions with carbon, nitrogen, phosphorous and oxygen nucleophiles. C60 reacts readily with organolithium and Grignard compounds to form alkyl, phenyl or alkanyl fullerenes. Possibly the most widely used additions to fullerene is the Bingel reaction (Figure 7.23), where a carbon nucleophile, generated by deprotonation of α-halo malonate esters or ketones, is added to form a cyclopropanation product. The α-halo esters and ketones can also be generated in situ with I_2 or CBr_4 and a weak base as 1,8-diazabicyclo[5.4.0]unde-7ene (DBU). The Bingel reaction is considered one of the most versatile and efficient methods to functionalize C_{60}.

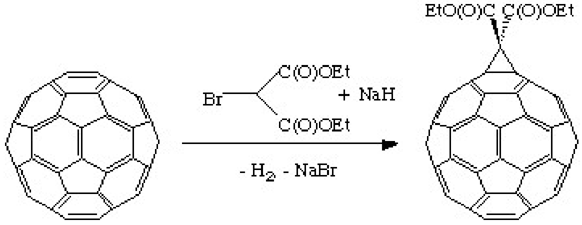

Figure 7.23: Bingel reaction of C_{60} with 2-bromoethylmalonate.

Cycloaddition is another powerful tool to functionalize fullerenes, in particular because of its selectivity with the 6,6 bonds, limiting the possible isomers (Figure 7.24). The dienophilic feature of the [6,6] double bonds of C_{60} enables the molecule to undergo various cycloaddition reactions in which the monoadducts can be generated in high yields. The best studies cycloadditon reactions of fullerene are [3+2] additions with diazoderivatives and azomethine ylides (Prato reactions). In this reaction, azomethine ylides can be generated *in situ* from condensation of α-amino acids with aldehydes or ketones, which produce 1,3 dipoles to further react with C_{60} in good yields (Figure 7.25). Hundreds of useful building blocks have been generated by those two methods. The Prato reactions have also been successfully applied to carbon nanotubes.

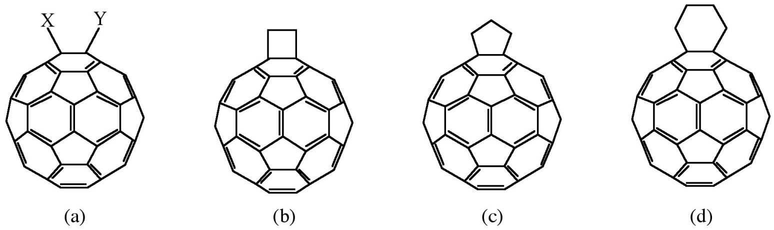

Figure 7.24: Geometrical shapes built onto a [6,6] ring junction: a) open, b) four-membered ring, c) five-membered ring, and d) six-membered ring.

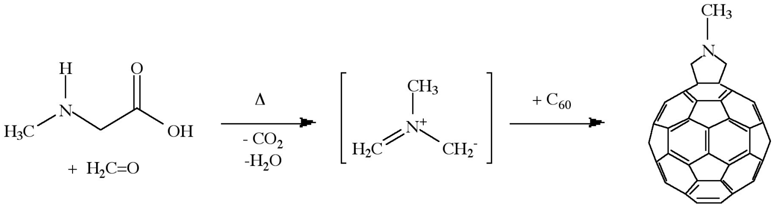

Figure 7.25: Prato reaction of C_{60} with N-methyglycine and paraformaldehyde.

The oxidation of fullerenes, such as C_{60}, has been of increasing interest with regard to applications in photoelectric devices, biological systems, and possible remediation of fullerenes. The oxidation of C_{60} to $C_{60}O_n$ (n = 1, 2) may be accomplished by photooxidation, ozonolysis, and epoxidation. With each of these methods, there is a limit to the isolable oxygenated product, $C_{60}O_n$ with $n < 3$. Highly oxygenated fullerenes, $C_{60}O_n$ with $3 \leq n \leq 9$, have been prepared by the catalytic oxidation of C_{60} with $ReMeO_3/H_2O_2$.

7.2.2.1.3 Carbon nanotubes

A key breakthrough in carbon nanochemistry came in 1993 with the report of needle-like tubes made exclusively of carbon. This material became known as carbon nanotubes (CNTs). There are several types of nanotubes. The first discovery was of multi walled tubes (MWNTs) resembling many pipes nested within each other. Shortly after MWNTs were discovered single walled nanotubes (SWNTs) were observed. Single walled tubes resemble a single pipe that is potentially capped at each end. The properties of single walled and multi walled tubes are generally the same, although single walled tubes are believed to have superior mechanical strength and thermal and electrical conductivity; it is also more difficult to manufacture them.

Single walled carbon nanotubes (SWNTs) are by definition fullerene materials. Their structure consists of a graphene sheet rolled into a tube and capped by half a fullerene (Figure 7.26). The carbon atoms in a SWNT, like those in a fullerene, are sp2 hybridized. The structure of a nanotube is analogous to taking this graphene sheet and rolling it into a seamless cylinder. The different types of SWNTs are defined by their diameter and chirality. Most of the presently used single-wall carbon nanotubes have been synthesized by the pulsed laser vaporization method, however, increasingly SWNTs are prepared by vapor liquid solid catalyzed growth.

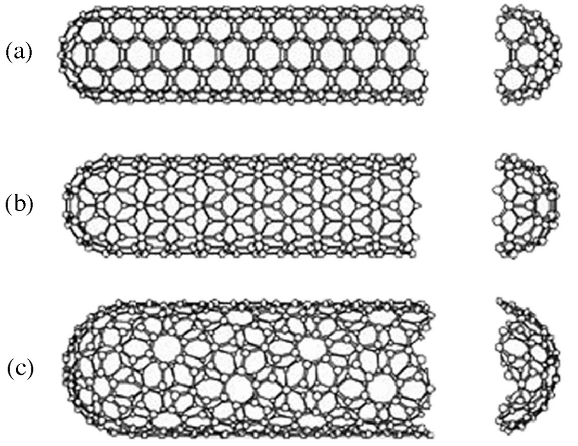

Figure 7.26: Structure of single walled carbon nanotubes (SWNTs) with (a) armchair, (b) zig-zag, and (c) chiral chirality.

The physical properties of SWNTs have made them an extremely attractive material for the manufacturing of nano devices. SWNTs have been shown to be stronger than steel as estimates for the Young's modulus approaches 1 Tpa. Their electrical conductance is comparable to copper with anticipate current densities of up to 10^{13} A/cm^2 and a resistivity as low as 0.34 x 10^{-4} Ω.cm at room temperatures. Finally, they have a high thermal conductivity (3000 - 6000 W.m/K).

The electronic properties of a particular SWNT structure are based on its chirality or twist in the structure of the tube which is defined by its n,m value. The values of n and m determine the chirality, or "twist" of the nanotube. The chirality in turn affects the conductance of the nanotube, its density, its lattice structure, and other properties. A SWNT is considered metallic if the value n-m is divisible by three. Otherwise, the nanotube is semi-conducting. The external environment also has an effect on the conductance of a tube, thus molecules such as O_2 and NH_3 can change the overall conductance of a tube, while the presence of metals have been shown to significantly effect the opto-electronic properties of SWNTs.

Multi walled carbon nanotubes (MWNTs) range from double walled NTs, through many-walled NTs (Figure 7.27) to carbon nanofibers. Carbon nanofibers are the extreme of multi walled tubes (Figure 7.28) and they are thicker and longer than either SWNTs or MWNTs, having a cross-sectional of ca. 500 Å^2 and are between 10 to 100 μm in length. They have been used extensively in the construction of high strength composites.

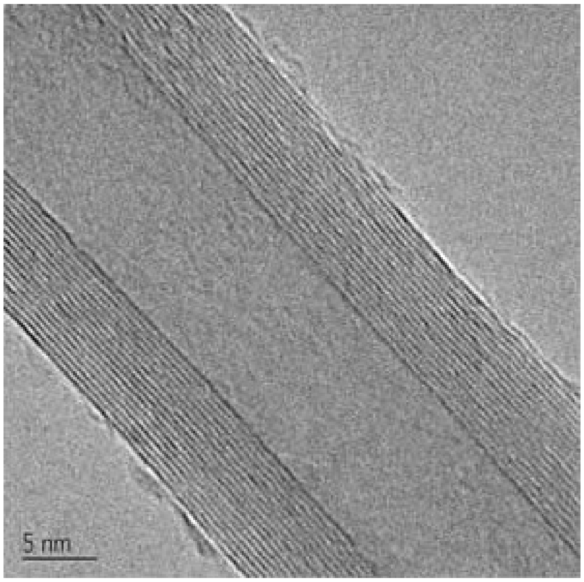

Figure 7.27: TEM image of an individual multi walled carbon nanotube (MWNTs). Copyright of Nanotech Innovations.

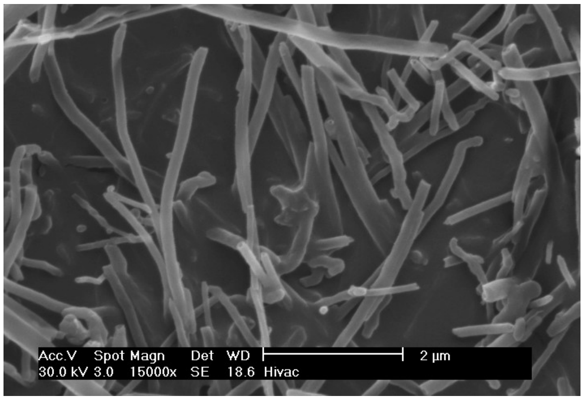

Figure 7.28: SEM image of vapor grown carbon nanofibers.

7.2.2.1.3.1 Synthesis of carbon nanotubes

A range of methodologies have been developed to produce nanotubes in sizeable quantities, including arc discharge, laser ablation, high pressure carbon monoxide (HiPco), and vapor liquid solid (VLS) growth. All these processes take place in vacuum or at low pressure with a process gases, although VLS growth can take place at atmospheric pressure. Large quantities of nanotubes can be synthesized by these methods; advances in catalysis and continuous growth processes are making SWNTs more commercially viable.

The first observation of nanotubes was in the carbon soot formed during the arc discharge production of fullerenes. The high temperatures caused by the discharge caused the carbon contained in the negative electrode to sublime and the CNTs are deposited on the opposing electrode. Tubes produced by this method were initially multi walled tubes (MWNTs). However, with the addition of cobalt to the vaporized carbon, it is possible to grow single walled nanotubes. This method it produces a mixture of components, and requires further purification to separate the CNTs from the soot and the residual catalytic metals. Producing CNTs in high yield depends on the uniformity of the plasma arc, and the temperature of the deposit forming on the carbon electrode.

Higher yield and purity of SWNTs may be prepared by the use of a dual-pulsed laser. SWNTs can be grown in a 50% yield through direct vaporization of a Co/Ni doped graphite rod with a high-powered laser in a tube furnace operating at 1200 °C. The material produced by this method appears as a mat of "ropes", 10 - 20 nm in diameter and up to 100 μm or more in length. Each rope consists of a bundle of SWNTs, aligned along a common axis. By varying the process parameters such as catalyst composition and the growth temperature, the average nanotube diameter and size distribution can be varied. Although arc-discharge and laser vaporization are currently the principal methods for obtaining small quantities of high quality SWNTs, both methods suffer from drawbacks. The first is that they involve evaporating the carbon source, making scale-up on an industrial level difficult and energetically expensive. The second issue relates to the fact that vaporization methods grow SWNTs in highly tangled forms, mixed with unwanted forms of carbon and/or metal species. The SWNTs thus produced are difficult to purify, manipulate, and assemble for building nanotube-device architectures for practical applications.

In order to overcome some of the difficulties of these high-energy processes, the chemical catalysis method was developed in which a hydrocarbon feedstock is used in combination with a metal catalyst. The catalyst is typically, but not limited to iron, colbalt, or iron/molybdenum, it is heated under reducing conditions in the presence of a suitable carbon feedstock, e.g., ethylene. This method can be used for both SWNTs and MWNTs; the formation of each is controlled by the identity of the catalyst and the reaction conditions. A convenient laboratory scale apparatus is available from Nanotech Innovations, Inc., for the synthesis of highly uniform, consistent, research sample that uses pre-weighed catalyst/carbon source ampoules. This system, allows for 200 mg samples of MWNTs to be prepared for research and testing. The use of CO as a feedstock, in place of a hydrocarbon, led to the development of the high-pressure carbon monoxide (HiPco) procedure for SWNT synthesis. By this method, it is possible to produce gram quantities of SWNTs, unfortunately, efforts to scale beyond that have not met with complete success.

Initially developed for small-scale investigations of catalyst activity, vapor liquid solid (VLS) growth of nanotubes has been highly studied, and now shows promise for large-scale production of nanotubes. Recent approaches have involved the use of well-defined nanoparticle or molecular precursors and many different transition metals have been employed, but iron, nickel, and cobalt remain to be the focus of most research. The nanotubes grow at the sites of the metal catalyst; the carbon-containing gas is broken apart at the surface of the catalyst particle, and the carbon is transported to the edges of the particle, where it forms the nanotube. The length of the tube grown in surface supported catalyst VLS systems appears to be dependent on the orientation of the growing tube with the surface. By properly adjusting the surface concentration and aggregation of the catalyst particles it is possible to synthesize vertically aligned carbon nanotubes, i.e., as a carpet perpendicular to the substrate.

Of the various means for nanotube synthesis, the chemical processes show the greatest promise for industrial scale deposition in terms of its price/unit ratio. There are additional advantages to the VLS growth, which unlike the other methods is capable of growing nanotubes directly on a desired substrate. The growth sites are controllable by careful deposition of the catalyst. Additionally, no other growth methods have been developed to produce vertically aligned SWNTs.

7.2.2.1.3.2 Chemical functionalization of carbon nanotubes

The limitation of using carbon nanotubes in any practical applications has been its solubility; for example SWNTs have little to no solubility in most solvent due to the aggregation of the tubes. Aggregation/roping of nanotubes occurs as a result of the high van der Waals binding energy of *ca.* 500 eV per mm of tube contact. The van der Waals force between the tubes is so great, that it take tremendous energy to pry them apart, making it very to make combination of nanotubes with other materials such as in composite applications. The functionalization of nanotubes, i.e., the attachment of "chemical functional groups" provides the path to overcome these barriers. Functionalization can improve solubility as well as processibility, and has been used to align the properties of nanotubes to those of other materials. The clearest example of this is the ability to solubilize nanotubes in a variety of solvents, including water. It is important when discussing functionalization that a distinction is made between covalent and non-covalent functionalization.

Current methods for solubilizing nanotubes without covalent functionalization include highly aromatic solvents, super acids, polymers, or surfactants. Non-covalent "functionalization" is generally on the concept of supramolecular interactions between the SWNT and some macromolecule as a result of various adsorption forces, such as van der Waals' and π-stacking interactions. The chemical speciation of the nanotube itself is not altered as a result of the interaction. In contrast, covalent functionalization relies on the chemical reaction at either the sidewall or end of the SWNT. As may be expected the high aspect ratio of nanotubes means that sidewall functionalization is much more important than the functionalization of the cap. Direct covalent sidewall functionalization is associated with a change of hybridization from sp^2 to sp^2 and a simultaneous loss of conjugation. An alternative approach to covalent functionalization involves the reaction of defects present (or generated) in the structure of the nanotube. Defect sites can be the open ends and holes in the sidewalls, and pentagon and heptagon irregularities in the hexagon graphene framework (often associated with bends in the tubes). All these functionalizations are exohedral derivatizations. Taking the hollow structure of nanotubes into consideration, endohedral functionalization of SWNTs is possible, i.e., the filling of the tubes with atoms or small molecules. It is important to note that covalent functionalization methods have one problem in common: extensive covalent functionalization modifies SWNT properties by disrupting the continuous π–system of SWNTs.

Various applications of nanotubes require different, specific modification to achieve desirable physical and chemical properties of nanotubes. In this regard, covalent functionalization provides a higher degree of fine-tuning the chemistry and physics of SWNTs than non-covalent functionalization. Until now, a variety of methods have been used to achieve the functionalization of nanotubes (Figure 7.29).

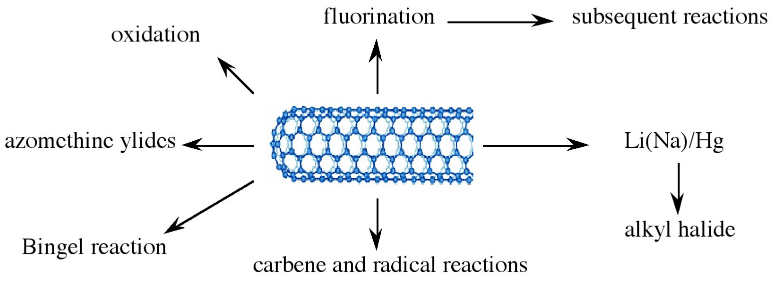

Figure 7.29: Schematic description of various covalent functionalization strategies for SWNTs.

Taking chemistry developed for C$_{60}$, SWNTs may be functionalized using 1,3 dipolar addition of azomethine ylides. The functionalized SWNTs are soluble in most common organic solvents. The azomethine ylide functionalization method was also used for the purification of SWNTs. Under electrochemical conditions, aryl diazonium salts react with SWNTs to achieve functionalized SWNTs, alternatively the diazonium ions may be generated *in-situ* from the corresponding aniline, while a solvent free reaction provides the best chance for large-scale functionalization this way. In each of these methods it is possible to control the amount of functionalization on the tube by varying reaction times and the reagents used; functionalization as high as 1 group per every 10 - 25 carbon atoms is possible.

Organic functionalization through the use of alkyl halides, a radical pathway, on tubes treated with lithium in liquid ammonia offers a simple and flexible route to a range of functional groups. In this reaction, functionalization occurs on every 17 carbons. Most success has been found when the tubes are dodecylated. These tubes are soluble in chloroform, DMF, and THF.

The addition of oxygen moieties to SWNT sidewalls can be achieved by treatment with acid or wet air oxidation, and ozonolysis. The direct epoxidation of SWNTs may be accomplished by the direct reaction with a peroxide reagent, or catalytically. Catalytic de-epoxidation (Figure 7.30) allows for the quantitative analysis of sidewall epoxide and led to the surprising result that previously assumed “pure” SWNTs actually contain *ca.* 1 oxygen per 250 carbon atoms.

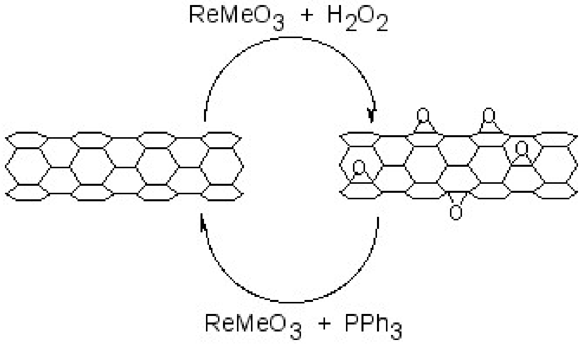

Figure 7.30: Catalytic oxidation and de-epoxidation of SWNTs.

One of the easiest functionalization routes, and a useful synthon for subsequent conversions, is the fluorination of SWNTs, using elemental fluorine. Importantly, a C:F ratios of up to 2:1 can be achieved without disruption of the tubular structure. The fluorinated SWNTs (F-SWNTs) proved to be much more soluble than pristine SWNTs in alcohols (1 mg/mL in *iso*-propanol), DMF and other selected organic solvents. Scanning tunneling microscopy (STM) revealed that the fluorine formed bands of approximately 20 nm, while calculations using DFT revealed 1,2 addition is more energetically preferable than 1,4 addition, which has been confirmed by solid state ^{13}C NMR. F-SWNTs make highly flexible synthons and subsequent elaboration has been performed with organo lithium, Grignard reagents, and amines.

Functionalized nanotubes can be characterized by a variety of techniques, such as atomic force microscopy (AFM), transmission electron microscopy (TEM), UV-vis spectroscopy, and Raman spectroscopy. Changes in the Raman spectrum of a nanotube sample can indicate if functionalization has occurred. Pristine tubes exhibit two distinct bands. They are the radial breathing mode (230 cm^{-1}) and the tangential mode (1590 cm^{-1}). When functionalized, a new band, called the disorder band, appears at *ca.*1350 cm^{-1}. This band is attributed to sp^3-hybridized carbons in the tube. Unfortunately, while the presence of a significant D mode is consistent with sidewall functionalization and the relative intensity of D (disorder) mode versus the tangential G mode (1550 – 1600 cm^{-1}) is often used as a measure of the level of substitution. However, it has been shown that Raman is an unreliable method for determination of the extent of functionalization since the relative intensity of the D band is also a function of the substituents distribution as well as concentration.

Recent studies suggest that solid state ^{13}C NMR are possibly the only definitive method of demonstrating covalent attachment of particular functional groups.

7.2.2.1.3.3 Coating carbon nanotubes: creating inorganic nanostructures

Fullerenes, nanotubes and nanofibers represent suitable substrates for the seeding other materials such as oxides and other minerals, as well as semiconductors. In this regard, the carbon nanomaterial acts as a seed point for the growth as well as a method of defining unusual aspect ratios. For example, silica fibers can be prepared by a number of methods, but it is only through coating SWNTs that silica nano-fibers with of micron lengths with tens of nanometers in diameter may be prepared.

While C_{60} itself does not readily seed the growth of inorganic materials, liquid phase deposition of oxides, such as silica, in the presence of fullerenol, $C_{60}(OH)_n$, results in the formation of uniform oxide spheres. It appears the fullerenol acts as both a reagent and a physical point for subsequent oxide growth, and it is C_{60}, or an aggregate of C_{60}, that is present within the spherical particle. The addition of fullerenol alters the morphology and crystal phase of $CaCO_3$ precipitates from aqueous solution, resulting in the formation of spherical features, 5-pointed flower shaped clusters, and triangular crystals as opposed to the usual rhombic crystals. In addition, the meta-stable vaterite phase is observed with the addition of $C_{60}(OH)_n$.

As noted above individual SWNTs may be obtained in solution when encased in a cylindrical micelle of a suitable surfactant. These individualized nanotubes can be coated with a range of inorganic materials. Liquid phase deposition (LPD) appears to have significant advantages over other methods such as incorporating surfacted SWNTs into a preceramic matrix, *in situ* growth of the SWNT in an oxide matrix, and sol-gel methods. The primary advantage of LPD growth is that individual SWNTs may be coated rather than bundles or ropes. For example, SWNTs have been coated with silica by liquid phase deposition (LPD) using a silica/H_2SiF_6 solution and a surfactant-stabilized solution of SWNTs. The thickness of the coating is dependent on the reaction mixture concentration and the reaction time. The SWNT core can be removed by thermolysis under oxidizing conditions to leave a silica nano fiber. It is interesting to note that the use of a surfactant is counter productive when using MWNTs and VGFs, in this case surface activation of the nanotube offers the suitable growth initiation. Pre-oxidation of the MWNT or VGF allows for uniform coatings to be deposited. The coated SWNTs, MWNTs, and VGFs can be subsequently reacted with suitable surface reagents to impart miscibility in aqueous solutions, guar gels, and organic matrixes. In addition to simple oxides, coated nanotubes have been prepared with minerals such as carbonates and semiconductors.

7.2.2.1.4 Bibliography

- S. M. Bachilo, M. S. Strano, C. Kittrell, R. H. Hauge, R. E. Smalley, and R. B. Weisman, *Science*, 2002, **298**, 2361.
- D. S. Bethune, C. H. Klang, M. S. deVries, G. Gorman, R. Savoy, J. Vazquez, and R. Beyers, *Nature*, 1993, **363**, 605.
- J, J. Brege, C. Gallaway, and A. R. Barron, *J. Phys. Chem., C*, 2007, **111**, 17812.
- C. A. Dyke and J. M. Tour, *J. Am. Chem. Soc.*, 2003, **125**, 1156.
- Z. Ge, J. C. Duchamp, T. Cai, H. W. Gibson, and H. C. Dorn, *J. Am. Chem. Soc.*, 2005, **127**, 16292.
- L. A. Girifalco, M. Hodak, and R. S. Lee, *Phys. Rev. B*, 2000, **62**, 13104.
- T. Guo, P. Nikolaev, A. G. Rinzler, D. Tománek, D. T. Colbert, and R. E. Smalley, *J. Phys. Chem.*, 1995, **99**, 10694.
- J. H. Hafner, M. J. Bronikowski, B. R. Azamian, P. Nikolaev, A. G. Rinzler, D. T. Colbert, K. A. Smith, and R. E. Smalley, *Chem. Phys. Lett.*, 1998, **296**, 195.
- A. Hirsch, *Angew. Chem. Int. Ed.*, 2002, **40**, 4002.
- S. Iijima and T. Ichihashi, *Nature*, 1993, **363**, 603.
- H. R. Jafry, E. A. Whitsitt, and A. R. Barron, *J. Mater. Sci.*, 2007, **42**, 7381.
- H. W. Kroto, J. R. Heath, S. C. O'Brien, R. F. Curl, and R. E. Smalley, *Nature*, 1985, **318**, 162.
- F. Liang, A. K. Sadana, A. Peera, J. Chattopadhyay, Z. Gu, R. H. Hauge, and W. E. Billups, *Nano Lett.*, 2004, **4**, 1257.

- D. Ogrin and A. R. Barron, *J. Mol. Cat. A: Chem.*, 2006, **244**, 267.
- D. Ogrin, J. Chattopadhyay, A. K. Sadana, E. Billups, and A. R. Barron, *J. Am. Chem. Soc.*, 2006, **128**, 11322.
- R. E. Smalley, *Acc. Chem. Res.*, 1992, **25**, 98.
- M. M. J. Treacy, T. W. Ebbesen, and J. M. Gibson, *Nature*, 1996, **381**, 678.
- E. A. Whitsitt and A. R. Barron, *Nano Lett.*, 2003, **3**, 775.
- J. Yang and A. R. Barron, *Chem. Commun.*, 2004, 2884.
- L. Zeng, L. B. Alemany, C. L. Edwards, and A. R. Barron, *Nano Res.*, 2008, **1**, 72.

7.2.2.2 Graphene[4]

7.2.2.2.1 Introduction

Graphene is a one-atom-thick planar sheet of sp^2-bonded carbon atoms that are densely packed in a honeycomb crystal lattice (Figure 7.31). The name comes from "graphite" and "alkene"; graphite itself consists of many graphene sheets stacked together.

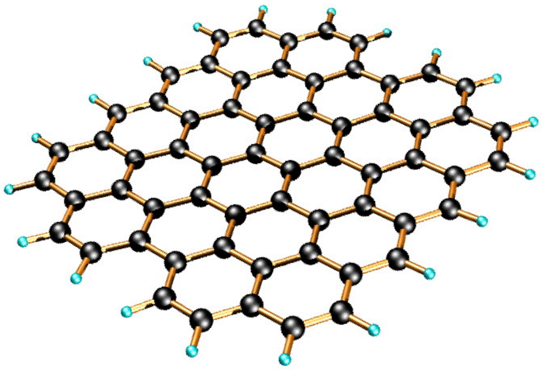

Figure 7.31: Idealized structure of a single graphene sheet.

Single-layer graphene nanosheets were first characterized in 2004, prepared by mechanical exfoliation (the "scotch-tape" method) of bulk graphite. Later graphene was produced by epitaxial chemical vapor deposition on silicon carbide and nickel substrates. Most recently, graphene nanoribbons (GNRs) have been prepared by the oxidative treatment of carbon nanotubes and by plasma etching of nanotubes embedded in polymer films.

7.2.2.2.2 Physical properties of graphene

Graphene has been reported to have a Young's modulus of 1 TPa and intrinsic strength of 130 GP; similar to single walled carbon nanotubes (SWNTs). The electronic properties of graphene also have some similarity with carbon nanotubes. Graphene is a zero-bandgap semiconductor. Electron mobility in graphene is extraordinarily high (15,000 $cm^2/V.s$ at room temperature) and ballistic electron transport is reported to be on length scales comparable to that of SWNTs. One of the most promising aspects of graphene involves

---

[4] This content is available online at <http://cnx.org/content/m29187/1.4/>.

the use of GNRs. Cutting an individual graphene layer into a long strip can yield semiconducting materials where the bandgap is tuned by the width of the ribbon.

While graphene's novel electronic and physical properties guarantee this material will be studied for years to come, there are some fundamental obstacles yet to overcome before graphene based materials can be fully utilized. The aforementioned methods of graphene preparation are effective; however, they are impractical for large-scale manufacturing. The most plentiful and inexpensive source of graphene is bulk graphite. Chemical methods for exfoliation of graphene from graphite provide the most realistic and scalable approach to graphene materials.

Graphene layers are held together in graphite by enormous van der Waals forces. Overcoming these forces is the major obstacle to graphite exfoliation. To date, chemical efforts at graphite exfoliation have been focused primarily on intercalation, chemical derivatization, thermal expansion, oxidation-reduction, the use of surfactants, or some combination of these.

7.2.2.2.3 Graphite oxide

Probably the most common route to graphene involves the production of graphite oxide (GO) by extremely harsh oxidation chemistry. The methods of Staudenmeier or Hummers are most commonly used to produce GO, a highly exfoliated material that is dispersible in water. The structure of GO has been the subject of numerous studies; it is known to contain epoxide functional groups along the basal plane of sheets as well as hydroxyl and carboxyl moieties along the edges (Figure 7.32). In contrast to other methods for the synthesis of GO, the the *m*-peroxybenzoic acid (*m*-CPBA) oxidation of microcrystalline synthetic graphite at room temperature yields graphite epoxide in high yield, without significant additional defects.

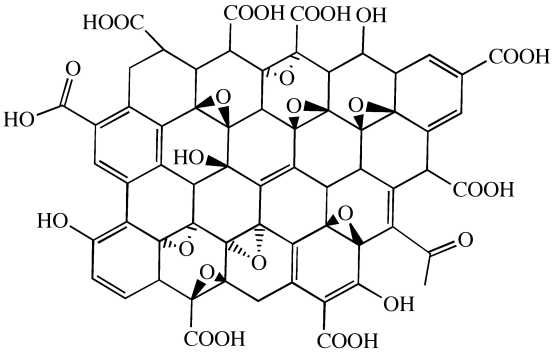

Figure 7.32: Idealized structure proposed for graphene oxide (GO). Adapted from C. E. Hamilton, PhD Thesis, Rice University (2009).

As graphite oxide is electrically insulating, it must be converted by chemical reduction to restore the electronic properties of graphene. Chemically converted graphene (CCG) is typically reduced by hydrazine or borohydride. The properties of CCG can never fully match those of graphene for two reasons:

1. Oxidation to GO introduces defects.
2. Chemical reduction does not fully restore the graphitic structure.

As would be expected, CCG is prone to aggregation unless stabilized. Graphene materials produced from pristine graphite avoid harsh oxidation to GO and subsequent (incomplete) reduction; thus, materials produced are potentially much better suited to electronics applications.

A catalytic approach to the removal of epoxides from fullerenes and SWNTs has been applied to graphene epoxide and GO. Treatment of oxidized graphenes with methyltrioxorhenium ($MeReO_3$, MTO) in the presence of PPh_3 results in the oxygen transfer, to form $O{=}PPh_3$ and allow for quantification of the C:O ratio.

7.2.2.2.4 Homogeneous graphene dispersions

An alternate approach to producing graphene materials involves the use of pristine graphite as starting material. The fundamental value of such an approach lies in its avoidance of oxidation to GO and subsequent (incomplete) reduction, thereby preserving the desirable electronic properties of graphene. There is precedent for exfoliation of pristine graphite in neat organic solvents without oxidation or surfactants. It has been reported that *N*,*N*-dimethylformamide (DMF) dispersions of graphene are possible, but no detailed characterization of the dispersions were reported. In contrast, Coleman and coworkers reported similar dispersions using *N*-methylpyrrolidone (NMP), resulting in individual sheets of graphene at a concentration of $\leq$0.01 mg/mL. NMP and DMF are highly polar solvents, and not ideal in cases where reaction chemistry requires a nonpolar medium. Further, they are hygroscopic, making their use problematic when water must be excluded from reaction mixtures. Finally, DMF is prone to thermal and chemical decomposition.

Recently, dispersions of graphene has been reported in *ortho*-dichlorobenzene (ODCB) using a wide range of graphite sources. The choice of ODCB for graphite exfoliation was based on several criteria:

1. ODCB is a common reaction solvent for fullerenes and is known to form stable SWNT dispersions.
2. ODCB is a convenient high-boiling aromatic, and is compatible with a variety of reaction chemistries.
3. ODCB, being aromatic, is able to interact with graphene *via* π-π stacking.
4. It has been suggested that good solvents for graphite exfoliation should have surface tension values of 40 – 50 mJ/m^2. ODCB has a surface tension of 36.6 mJ/m^2, close to the proposed range.

Graphite is readily exfoliated in ODCB with homogenization and sonication. Three starting materials were successfully dispersed: microcrystalline synthetic, thermally expanded, and highly ordered pyrolytic graphite (HOPG). Dispersions of microcrystalline synthetic graphite have a concentration of 0.03 mg/mL, determined gravimetrically. Dispersions from expanded graphite and HOPG are less concentrated (0.02 mg/mL).

High resolution transmission electron microscopy (HRTEM) shows mostly few-layer graphene ($n < 5$) with single layers and small flakes stacked on top (Figure 7.33). Large graphitic domains are visible; this is further supported by selected area electron diffraction (SAED) and fast Fourier transform (FFT) in selected areas. Atomic force microscope (AFM) images of dispersions sprayed onto silicon substrates shows extremely thin flakes with nearly all below 10 nm. Average height is 7 - 10 nm. The thinnest are less than 1 nm, graphene monolayers. Lateral dimensions of nanosheets range from 100 – 500 nm.

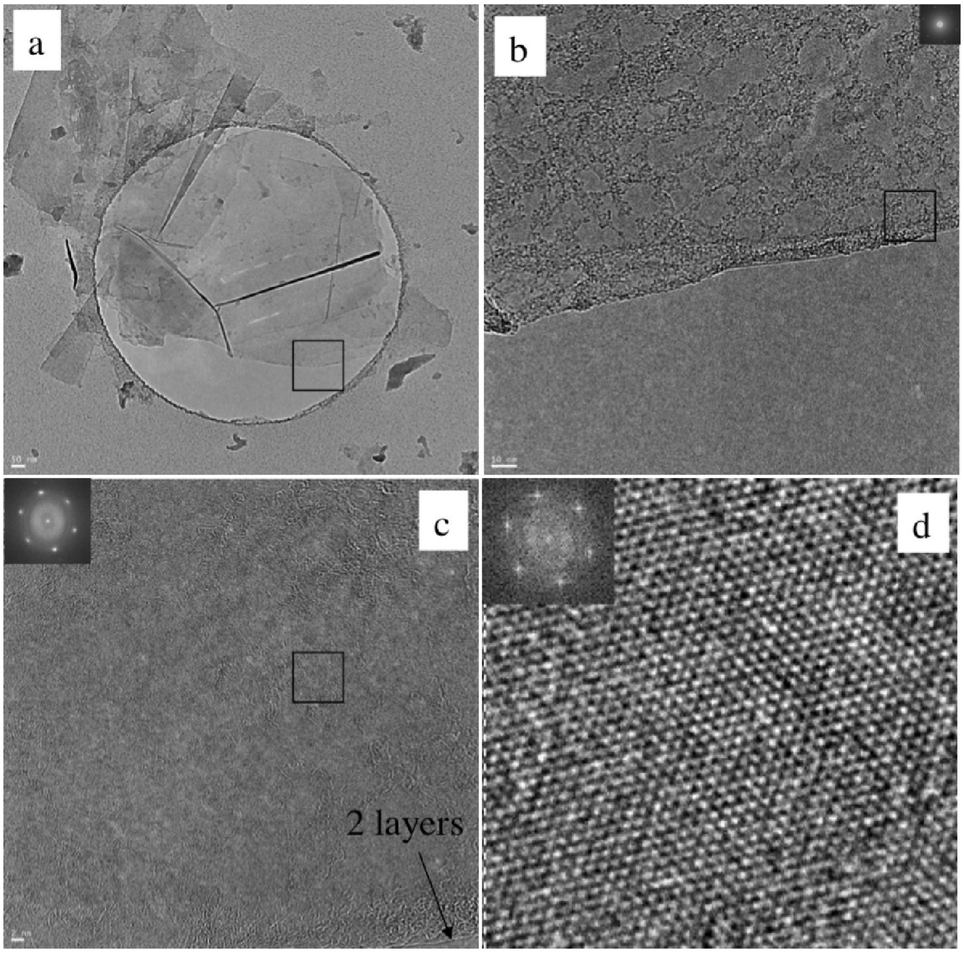

Figure 7.33: TEM images of single layer graphene from HOPG dispersion. (a) monolayer and few layer of graphene stacked with smaller flakes; (b) selected edge region from (a), (c) selected area from (b) with FFT inset, (d) HRTEM of boxed region in (c) showing lattice fringes with FFT inset. Adapted from C. E. Hamilton, PhD Thesis, Rice University (2009).

As-deposited films cast from ODCB graphene show poor electrical conductivity, however, after vacuum annealing at 400 °C for 12 hours the films improve vastly, having sheet resistances on the order of 60 Ω/sq. By comparison, graphene epitaxially grown on Ni has a reported sheet resistance of 280 Ω/sq.

7.2.2.2.5 Covalent functionalization of graphene and graphite oxide

The covalent functionalization of SWNTs is well established. Some routes to covalently functionalized SWNTs include esterification/ amidation, reductive alkylation (Billups reaction), and treatment with azomethine ylides (Prato reaction), diazonium salts, or nitrenes. Conversely, the chemical derivatization of graphene and GO is still relatively unexplored.

Some methods previously demonstrated for SWNTs have been adapted to GO or graphene. GO carboxylic acid groups have been converted into acyl chlorides followed by amidation with long-chain amines.

Additionally, the coupling of primary amines and amino acids via nucleophilic attack of GO epoxide groups has been reported. Yet another route coupled isocyanates to carboxylic acid groups of GO. Functionalization of partially reduced GO by aryldiazonium salts has also been demonstrated. The Billups reaction has been performed on the intercalation compound potassium graphite (C_8K), as well as graphite fluoride, and most recently GO. Graphene alkylation has been accomplished by treating graphite fluoride with alkyllithium reagents.

ODCB dispersions of graphene may be readily converted to covalently functionalize graphene. Thermal decomposition of benzoyl peroxide is used to initiate radical addition of alkyl iodides to graphene in ODCB dispersions.

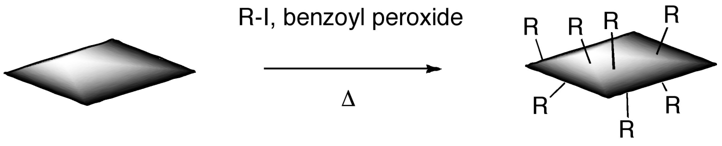

(7.12)

Additionally, functionalized graphene with nitrenes generated by thermal decomposition of aryl azides

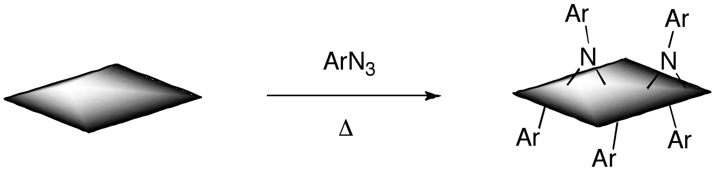

(7.13)

7.2.2.2.6 Bibliography

- P. Blake, P. D. Brimicombe, R. R. Nair, T. J. Booth, D. Jiang, F. Schedin, L. A. Ponomarenko, S. V. Morozov, H. F. Gleeson, E. W. Hill, A. K. Geim, and K. S. Novoselov, *Nano Lett.*, 2008, **8**, 1704.
- J. Chattopadhyay, A. Mukherjee, C. E. Hamilton, J.-H. Kang, S. Chakraborty, W. Guo, K. F. Kelly, A. R. Barron, and W. E. Billups, *J. Am. Chem. Soc.*, 2008, **130**, 5414.
- G. Eda, G. Fanchini, and M. Chhowalla, *Nat. Nanotechnol.*, 2008, **3**, 270.
- M. Y. Han, B. Ozyilmaz, Y. Zhang, and P. Kim, *Phys. Rev. Lett.*, 2008, **98**, 206805.
- Y. Hernandez, V. Nicolosi, M. Lotya, F. M. Blighe, Z. Sun, S. De, I. T. McGovern, B. Holland, M. Byrne, Y. K. Gun'Ko, J. J. Boland, P. Niraj, G. Duesberg, S. Krishnamurthy, R. Goodhue, J. Hutchinson, V. Scardaci, A. C. Ferrari, and J. N. Coleman, *Nat. Nanotechnol.*, 2008, **3**, 563.
- W. S. Hummers and R. E. Offeman, *J. Am. Chem. Soc.*, 1958, **80**, 1339.
- L. Jiao, L. Zhang, X. Wang, G. Diankov, and H. Dai, *Nature*, 2009, **458**, 877.
- D. V. Kosynkin, A. L. Higginbotham, A. Sinitskii, J. R. Lomeda, A. Dimiev, B. K. Price, and J. M. Tour, *Nature*, 2009, **458**, 872.
- D. Li, M. B. Mueller, S. Gilje, R. B. Kaner, and G. G. Wallace, *Nat. Nanotechnol.*, 2008, **3**, 101.
- S. Niyogi, E. Bekyarova, M. E. Itkis, J. L. McWilliams, M. A. Hamon, and R. C. Haddon, *J. Am. Chem. Soc.*, 2006, **128**, 7720.
- Y. Si and E. T. Samulski, *Nano Lett.*, 2008, **8**, 1679.
- L. Staudenmaier, *Ber. Dtsch. Chem. Ges.*, 1898, **31**, 1481.

7.2.3 Nitrogen Compounds of Carbon[5]

There are a myriad of organic compounds containing carbon-nitrogen bonds, including: amines, imines, and nitriles. However, here we are concerned with the simplest carbon-nitrogen compounds.

---

[5] This content is available online at <http://cnx.org/content/m33075/1.3/>.

7.2.3.1 Cyanogen

Cyanogen, $(CN)_2$, may be considered the smallest molecular fragment containing carbon and nitrogen (Figure 7.34a). The reaction chemistry of cyanogen is related to that of the halogens, i.e., F_2, Cl_2, etc. Consequently, cyanogen is called a *pseudo halogen*.

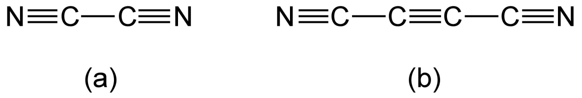

Figure 7.34: The structures of (a) cyanogen, $(CN)_2$ and (b) dicyanoacetylene (carbon subnitride, C_4N_2).

As shown in Table 7.7 the bonding in cyanogen is consistent with localization of the π-bonding between carbon and nitrogen given the similarity of the C-N bond distance in cyanogens and acetonitrile. However, there is clearly some π-delocalization associated with the C-C distance given its shortening as compared to ethane.

Compound	**Formula**	**C-C bond distance (Å)**	**C-N bond distance (Å)**
Cyanogen	$(CN)_2$	1.393	1.163
Hydrogen cyanide	HCN	-	1.154
Acetonitrile	CH_3CN	1.46	1.16
Ethane	C_2H_6	1.535	-
Ethylene	C_2H_4	1.339	-

Table 7.7: A comparison of the bond distances in selected carbon nitrogen compounds.

Cyanogen is produced by the reaction of a mixture of the cyanide and chloride of mercury, (7.14).

$$Hg(CN)_2 + HgCl_2 \rightarrow (CN)_2 + 2\,Hg + Cl_2 \tag{7.14}$$

Alternatively, the decomposition of unstable copper(II) cyanide, formed from a copper(II) salts with a Group 1 cyanide, (7.15), yields cyanogens, (7.16).

$$CuSO_4 + 2\,KCN \rightarrow Cu(CN)_2 + K_2SO_4 \tag{7.15}$$

$$2\,Cu(CN)_2 \rightarrow (CN)_2 + 2\,CuCN \tag{7.16}$$

Cyanogen is a flammable gas (Mp = -28 °C and Bp = -21 °C) that produces the second hottest flame natural flame (after carbon subnitride, C_4N_2) with a temperature of over 4525 °C when burnt in oxygen. Heating cyanogen in the absence of oxygen results self polymerizes, (7.17).

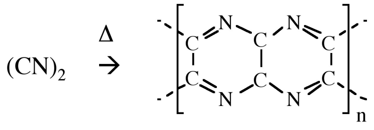

(7.17)

Hydrolysis of cyanogen results in addition across the carbon-nitrogen triple bonds and the formation of oxamide, (7.18). Cleavage of the C-C bond does occur in the presence of base (e.g., KOH), with the formation of cyanide (CN^-) and cyanate (CNO^-) salts, (7.19).

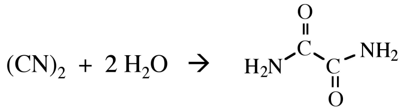

$$(CN)_2 + 2\,H_2O \rightarrow H_2N\text{-}C(=O)\text{-}C(=O)\text{-}NH_2 \qquad (7.18)$$

$$(CN)_2 + 2\,OH^- \rightarrow CN^- + CNO^- + H_2O \qquad (7.19)$$

7.2.3.2 Dicyanoacetylene

Dicyanoacetylene (also known as carbon subnitride or by its IUPAC name but-2-ynedinitrile) has the structure shown in Figure 7.34b, and may be thought of as a dicyanaide substituted acetylene.

At room temperature, dicyanoacetylene is a clear liquid, however, solid dicyanoacetylene has been detected in the atmosphere of Titan (the largest moon of the planet Saturn) by infrared spectroscopy. Dicyanoacetylene is an entropic explosive giving carbon powder and nitrogen gas. In the presence of oxgyen it burns with a bright blue-white flame at a temperature of 4990 °C.

7.2.3.3 Hydrogen cyanide

Hydrogen cyanide (HCN) is a colorless, highly poisonous, gas (Mp = -13.5 °C and Bp = 25.6 °C). Due to its original isolation from Prussian blue (hydrated ferric ferrocyanide), hydrogen cyanaide is also known by the name of *prussic acid*.

The synthesis of hydrogen cyanide is accomplished commercially by the partial oxidation of methane in the presence of ammonia, (7.20), using a platinum catalyst. The heat to activate the reaction is derived from the partial combustion of the methane and ammonia. The resulting aqueous solution is dried by distilled from phosphorus pentoxide (P_2O_5) to yield anhydrous hydrogen cyanide.

$$2\,CH_4 + 3\,O_2 + 2\,NH_3 \rightarrow 2\,HCN + 6\,H_2O \qquad (7.20)$$

Hydrogen cyanide may also be formed in the absence of oxygen, (7.21); however, in this case the reaction must be heated externally.

$$CH_4 + NH_3 \rightarrow HCN + 3\,H_2 \qquad (7.21)$$

Small quantities of hydrogen cyanide for laboratory use may be prepared by the reaction of an acid with a cyanide salt (either potassium or sodium), (7.22).

$$KCN + H^+ \rightarrow HCN + K^+ \qquad (7.22)$$

The structure of hydrogen cyanide is shown in Figure 7.35 along with its isomeric form, hydrogen isocyanide (HNC). While hydrogen cyanide is present in the pits of many fruits, and is generated by burnet moths and some millipedes, hydrogen isocyanide is only found in interstellar space. It is postulated, however, that along with HCN, HNC is an important building block for amino acids and hence life.

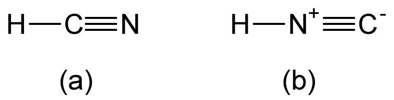

Figure 7.35: The structures of (a) hydrogen cyanaide (HCN) and (b) its isomer hydrogen isocyanide (HNC).

In the liquid state hydrogen cyanide forms strong hydrogen bonds (Figure 7.36). Hydrogen cyanide is a good solvent for polar compounds due to its high permittivity ($\in_r$) and high dipole moment (2.98 D).

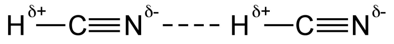

Figure 7.36: The hydrogen bonding in liquid hydrogen cyanide.

In aqueous solution hydrogen cyanide is a weak acid, (7.23), and several salts are known. However, HCN also reacts with water to give ammonium formate via formamide, (7.24).

$$HCN + H_2O \rightleftharpoons H_3O^+ + CN^- \tag{7.23}$$

$$HCN + H_2O \rightarrow HC(O)NH_2 \xrightarrow{H_2O} HCO_2^- + NH_4^+ \tag{7.24}$$

In a similar manner to cyanogen's relationship to the halogens, the cyanide anion (CN^-) is considered a *pseudo halide* (i.e., F^-, Cl^-, etc), and as such forms many coordination compounds, e.g., $[Fe(CN)_6]^{3-}$ and $[Ag(CN)_2]^-$.

7.2.3.3.1 Assassination, execution, and the Holocaust

Hydrogen cyanide is fatal to humans due to its inhibition of the enzyme cytochrome c oxidase by the cyanide ion (CN^-), which results in the halting of cellular respiration. A concentration of 300 mg/m^3 will kill within 10 minutes, while 3200 mg/m^3 (*ca.* 3500 ppm) will be fatal in about 1 minute.

The symptoms of cyanide poisoning appear similar to a heart attack and this has led to it being the poison of choice for both fictional murder mystery writers as well as the former KGB (*Konitet gosudarstvennoy bezopasnosti* or Committee for State Security) and its predecessor SMERSH (from the contraction *smert shpionam* meaning *death to spies*) in real life. Possibly the most famous use of hydrogen cyanide for assassination was the use of an atomizer mist gun by KGB agent Bohdan Stashynsky for the killing of the Ukranian political writer and anti-communist Lev Rebet in 1957, and later in 1959 that of fellow Ukranian, Stepan Bandera. In both cases the intention was to induce cardiac arrest and make it look like the victim had died of a heart attack.

Without doubt the most notorious use of hydrogen cyanide is in the form of the product Zyklon B, which was originally developed as an insecticide. Dr. Walter Heerdt found that hydrogen cyanide could be absorbed onto substrates such as absorbent pellets (e.g., silica), fibers, or diatomaceous earth (Figure 7.37). While stable in an airtight container, once opened the hydrogen cyanide is released. The "B" in the trade name comes from the German name for prussic acid (the common name for hydrogen cyanide), i.e., *Blausäure* meaning *blue acid.*

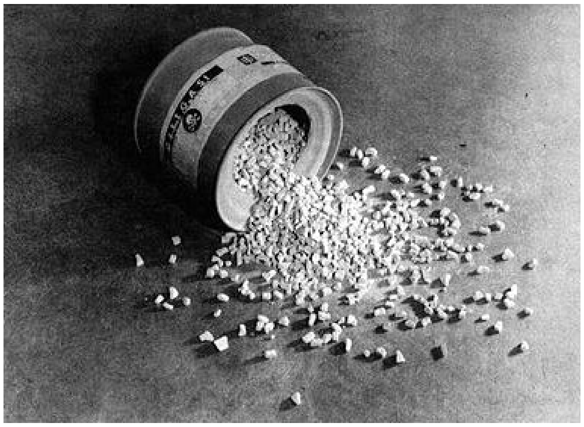

Figure 7.37: A can of Zyklon B granules.

The first wholesale use of Zyklon B was actually in the US where it was used as early as 1929 to disinfect the freight trains and cloths of Mexican immigrants entering the US. The first use of Zyklon B in the concentration camps during World War II was for a similar purpose (in particular for delousing to control typhus); however, for its use as an insecticide, Zyklon B contained a warning odorant. The deliberate manufacture of Zyklon B without the odorant resulted in the material that was used on a group of 250 gypsy children at the Buchenwald concentration camp in early 1940. Subsequently in September 1940, a similar number of sick Polish prisoners of war and 600 Soviet prisoners of war were killed at Auschwitz (Figure 7.38). Once these horrific tests were performed, the systematic murder of millions of people, including Jews, gypsies, and homosexuals, was accomplished using Zyklon B at Auschwitz, Majdanek, Sachsenhausen, and one of the Operation Reinhard camps. It is only fitting that many of the architects of the Holocaust themselves died from cyanide, including: Adolf Hitler (in addition to a bullet), Joseph Goebbles, Hermann Göring, and Heinrich Himmler.